

Università degli Studi di Milano

Facoltà di Scienze Matematiche, Fisiche e Naturali
Laurea Triennale in Fisica



Quantized Lubricant Velocity in a Bi-Dimensional Sliding Model

Relatore: Dott. Nicola Manini

Correlatore: Dott. Rosario Capozza

Ivano Eligio Castelli

Matricola n° 671951

A.A. 2006/2007

Codice PACS: 46.55.d

Quantized Lubricant Velocity in a Bi-Dimensional Sliding Model

Ivano Eligio Castelli

Dipartimento di Fisica, Università degli Studi di Milano,
Via Celoria 16, 20133 Milano, Italia

October 25, 2007

Abstract

Within the idealized scheme of a 1-dimensional Frenkel-Kontorova-like model, a special "quantized" sliding state was found for a solid lubricant confined between two periodic layers [1]. This state, characterized by a non-trivial geometrically fixed ratio of the mean lubricant drift velocity $\langle v_{\text{cm}} \rangle$ and the externally imposed translational velocity v_{ext} , was understood as due to the kinks (or solitons), formed by the lubricant due to incommensurability with one of the substrates, pinning to the other sliding substrate.

A quantized sliding state of the same nature is demonstrated here for a substantially less idealized 2-dimensional model, where atoms are allowed to move perpendicularly to the sliding direction and interact via Lennard-Jones potentials. Evidence for quantized sliding at finite temperature is provided, even with a solid confined lubricant composed of multiple (up to 7) lubricant layers. Characteristic backward lubricant motion produced by the presence of "anti-kinks" is also shown in this more realistic context.

Advisor: *Dr. Nicola Manini*

Co-Advisor: *Dr. Rosario Capozza*

Contents

1	Introduction	5
2	The 2D Model	5
3	Technical Implementation	8
3.1	Boundary Conditions	9
3.2	Simulation Time	10
4	The Plateau Dynamics	11
4.1	Single Lubricant Layer	11
4.2	Two Lubricant Layers and Varied Kink Coverage	17
4.3	Lubricant Multi-Layers	22
4.4	Anti-Kinks	26
5	Hysteresis	26
6	Analysis of the Fluctuations	31
7	Discussion and Conclusion	36
	Bibliography	38

1 Introduction

The problem of lubricated friction is a fascinating one, both from the fundamental point of view and for applications. Lubricants range from thick liquid layers to few or even single mono-layers, often in a solid or quasi-solid phase. In the present work, we address the effects of commensuration of the lubricant and the substrate surfaces. Perfect inter-atomic matching tends to produce locking, while sliding is favored by "defective" points, which can be introduced precisely by incommensuration of the lubricant and the sliding substrate lattice parameters. This lattice mismatch produces, in particular, special "quantized" sliding regime, where the sliding mean lubricant velocity, is fixed to an exact fraction of the substrate sliding velocity. This velocity fraction, in turn, is a simple function of the lubricant coverage of the more commensurate between the two substrate surfaces [2, 3]. This special sliding mode was discovered and analyzed in detail in a very idealized 1D Frenkel-Kontorova (FK)-like model [2]: the plateau mechanism was interpreted in terms of solitons, or kinks, being produced by the mismatch of the lubricant periodicity to that of one of the more commensurate substrate, with these kinks being dragged by the other, less commensurate, substrate.

In the present work, we investigate the presence of similar plateau associated to similar solitonic mechanisms in a slightly more realistic geometry: a 2D model of Lennard-Jones (LJ) atoms.

2 The 2D Model

We represent the sliding solid surface by rows of equally-spaced atoms; between these two "fixed" layer, we insert one or more layers of lubricant atoms (Fig. 1). Every layer is composed by equal particles that we take of unit mass ($m = 1$). While the reciprocal position of top and bottom substrate atoms are fixed, the atoms composing the lubricant layers can move freely under the action of pairwise Lennard-Jones interactions between lubricant atoms and between the lubricant atoms and the ones that compose the top and the bottom layers. For the LJ interaction energy, we consider the expression

$$\Phi_{\text{LJ}}(r) = \epsilon \left[\left(\frac{\sigma}{r} \right)^{12} - 2 \left(\frac{\sigma}{r} \right)^6 \right]. \quad (1)$$

This potential has an attractive tail at large- r , it reaches a minimum at σ and it turns repulsive at shorter distance. The potential (1) has an infinite range but for

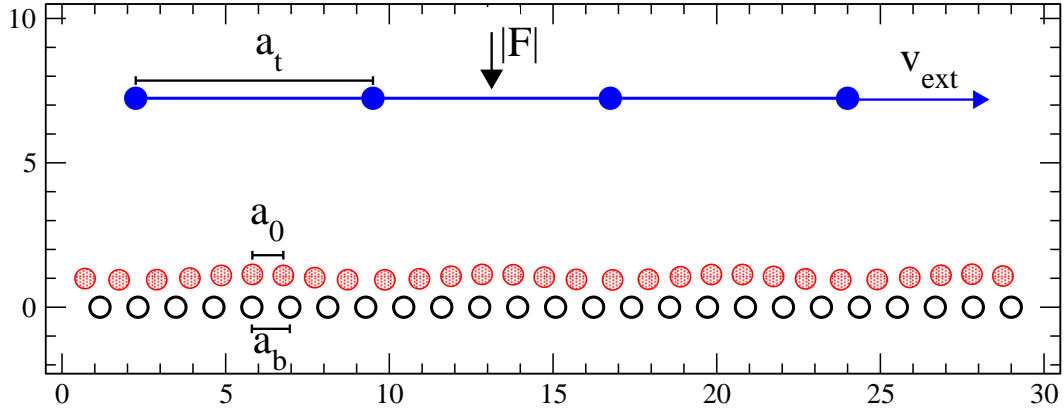


Figure 1: A sketch of the model with the rigid top (solid circles) and the bottom (open) layers (of lattice spacing a_t and a_b respectively). One (here) or more lubricant layers (shaded) or rest equilibrium spacing a_0 are confined in between.

practical purposes we introduce a cutoff radius R_C and disregard the interactions between atoms separated by more than R_C . But a simple truncation of the potential would create a problem: when a particle pair crosses the cutoff radius, the associated energy makes a jump; a large number of these jumps would spoil energy conservation in a simulation. To solve this problem, we shift the 2-body potential energy and eliminate the energy discontinuity as follows:

$$\Phi(r) = \begin{cases} \Phi_{\text{LJ}}(r) - \Phi_{\text{LJ}}(R_C) & r < R_C \\ 0 & r > R_C \end{cases}. \quad (2)$$

We set a cutoff radius $R_C = 2.5\sigma$, where $\Phi_{\text{LJ}}(R_C) \simeq -8.175 \cdot 10^{-3} \epsilon$.

The motion of the j -th lubricant particle is ruled by the following equation:

$$m \ddot{\vec{r}}_j = - \sum_{i_t=1}^{N_t} \frac{\partial}{\partial \vec{r}_j} \Phi^{\text{t,p}}(|\vec{r}_j - \vec{r}_{i_t}|) + \sum_{j'=1, j' \neq j}^{N_p} \frac{\partial}{\partial \vec{r}_j} \Phi^{\text{p,p}}(|\vec{r}_j - \vec{r}_{j'}|) - \sum_{i_b=1}^{N_b} \frac{\partial}{\partial \vec{r}_j} \Phi^{\text{b,p}}(|\vec{r}_j - \vec{r}_{i_b}|) \quad (3)$$

where \vec{r}_j is the position of the lubricant j -particle; r_{i_t} and r_{i_b} are the positions of top and bottom atoms; N_b , N_p and N_t are the numbers of bottom, lubricant and top particles; $\Phi^{\text{b,p}}$, $\Phi^{\text{p,p}}$ and $\Phi^{\text{t,p}}$ are the truncated 2-body potential energy for the interactions between bottom-lubricant, lubricant-lubricant and top-lubricant particles, respectively; finally

$$\frac{\partial}{\partial \vec{r}_j} \Phi(|\vec{r}_j - \vec{r}_{j'}|) = \frac{\vec{r}_j - \vec{r}_{j'}}{|\vec{r}_j - \vec{r}_{j'}|} \left. \frac{\partial \Phi(r)}{\partial r} \right|_{r=|\vec{r}_j - \vec{r}_{j'}|}. \quad (4)$$

By convention, we choose the frame of reference where the bottom layer is static. The top layer can move rigidly at a fixed horizontal velocity v_{ext} ; it can also move along the z -axis (its inertia equals the total mass of its atoms) under the external force F applied on each particle in the layer and under the force due to the interaction between the particles of the lubricant-layer and the top itself. Thus the dynamics of i_t -th particle of the top layer is described by the following equations:

$$r_{x_{i_t}}^{\text{top}}(t) = i_t a_t + v_{\text{ext}} t , \quad (5)$$

$$N_t m \ddot{r}_{z_{i_t}}^{\text{top}}(t) + \sum_{i_t=1}^{N_t} \sum_{j=1}^{N_p} \frac{\partial}{\partial r_z} \Phi^{\text{t,p}}(|\vec{r}_{i_t} - \vec{r}_j|) + N_t F = 0 \quad (6)$$

where $r_{x_j}^{\text{top}}$ and $r_{z_j}^{\text{top}}$ are the component of r^{top} along x and z , respectively. As all equations for $r_{z_j}^{\text{top}}$ are equal, irrespective of i_t , in practice the solution is unique $r_{z_j}^{\text{top}} \equiv r_z^{\text{top}}$.

Our simulations are made at fixed temperature. In order to keep the temperature at a fixed value, we use a Nosé-Hoover thermostat chain [4]. As shown in Ref. [5], the Nosé-Hoover chain method is described by the following equations:

$$m \ddot{\vec{r}}_j = F_j - \xi_1 m \dot{\vec{r}}_j , \quad (7)$$

$$\dot{\xi}_1 = \frac{1}{Q_1} \left(\sum_{i=1}^{N_p} |\dot{\vec{r}}_i|^2 - g K_B T \right) - \xi_1 \xi_2 , \quad (8)$$

$$\dot{\xi}_i = \frac{1}{Q_i} (Q_{i-1} \xi_{i-1}^2 - K_B T) - \xi_i \xi_{i+1} , \quad (9)$$

$$\dot{\xi}_M = \frac{1}{Q_M} (Q_{M-1} \xi_{M-1}^2 - K_B T) , \quad (10)$$

with $1 \leq j \leq N_p$ and $1 \leq i \leq M$, where M is the number of thermostats, that we take $M = 3$; we take Q_i , the effective "mass" of the each thermostat, and the coefficient g of the same order of N_p ; ξ_i is an auxiliary variable that keep the kinetic energy of the system close to its classical value $N_p K_B T$; F_j is the right side of Eq. (3). In our discussion, we take all $Q_i = m_{\text{therm}} = N_p$ and $g = 2(N_p - 1)$. We measure the thermal energy scale $K_B T$ in units of the LJ energy ϵ .

We assume, in general, to have three different sort of atoms, characterized by three lattice spacings, that, by convention, determine also the widths σ of LJ potential:

$$a_t = \sigma^{\text{tp}} , \quad a_0 = \sigma^{\text{pp}} \quad \text{and} \quad a_b = \sigma^{\text{bp}} , \quad (11)$$

defining the fixed and initial distances between neighboring substrate and lubricant atoms, respectively. These three different periodicities a_t , a_0 and a_b define

Physical quantity	Natural units
length	a_0
mass	m
energy	ϵ
force	ϵa_0^{-1}
velocity v	$\epsilon^{1/2} m^{-1/2}$
time	$m^{1/2} \epsilon^{-1/2} a_0$

Table 1: Natural units for several physical quantities in a system where length, mass and energy are measured in units of a_0 , m , ϵ .

two independent ratios:

$$r_t = \frac{a_t}{a_0}, \quad r_b = \frac{a_b}{a_0}. \quad (12)$$

For simplicity, we fix the same energy of interaction $\epsilon_{tp} = \epsilon_{pp} = \epsilon_{bp} = \epsilon$ for all pairwise coupling terms. We take this ϵ as energy unit, as well as a_0 as length unit and the mass m of all particles as mass unit. This choice defines a set of "natural" units for all physical quantities, which are implicitly defined in terms of these basic units. All quantities will then be expressed as dimensionless numbers, understanding that their value is referred to the natural units. To obtain a physical quantity in its explicit dimensional form, one should multiply its numerical value by the corresponding natural units listed in Table 1.

3 Technical Implementation

To solve the differential equations of motion (3, 6), we map them into a first-order problem of double size, and use a standard fourth-order Runge-Kutta method [6]. The classical Euler method to solve an equation $\frac{dy}{dt} = f(t, y)$ is based on the formula

$$y_{n+1} = y_n + hf(t_n, y_n) \quad (13)$$

(where h is the integration time-step) which suffers from an error $O(h^2)$. The Runge-Kutta method improves over the Euler method by implementing three more evaluation of $f(t, y)$. In fact, by evaluating more points in the interval $(t, t + h)$ it is possible to reduce the error by means of a suitably weighed average

over the different values of y obtained. The equation we employ are the following:

$$k_1 = hf(t_n, y_n) , \quad (14)$$

$$k_2 = hf\left(t_n + \frac{h}{2}, y_n + \frac{k_1}{2}\right) , \quad (15)$$

$$k_3 = hf\left(t_n + \frac{h}{2}, y_n + \frac{k_2}{2}\right) , \quad (16)$$

$$k_4 = hf(t_n + h, y_n + k_3) , \quad (17)$$

$$y_{n+1} = y_n + \frac{1}{6}(k_1 + 2k_2 + 2k_3 + k_4) + O(h^5) . \quad (18)$$

In this scheme, k_1 is the slope at the beginning of the interval; k_2 is the slope at the midpoint of the interval, using slope k_1 to determine the value of y at the point $t_n + \frac{h}{2}$ using Euler's method; k_3 is the slope at the midpoint, but now using the slope k_2 to determine the y -value and k_4 is the slope at the end of the interval, with its y -value determined using k_3 . This high-order method is extremely accurate, and we check all our results by comparing two different time step h .

3.1 Boundary Conditions

The number of atoms N of the simulated system is negligible compared with a realistic number of atoms at the surface of contact of a macroscopic piece of matter (easily of the order of 10^{11} in a mm^2): this produces unphysical boundary effects in the simulations. To alleviate this problem, we use *periodic boundary conditions* (PBC): particles are enclosed in a box replicated infinitely by means of rigid translation. Thus, if a particle is located at position r in the box, we assume that this particle really represents an infinite set of particles located at $r + nL$, where n runs over all possible integer numbers and L is the vector corresponding to the edge of the box. All these "image" particles move together and, in fact, only one copy of each of them is represented in the computer program, but each particle j in the box should be thought as interacting not only with other particles j' in the box, but also with their images in nearby boxes.

We check for effects of the PBC by means of standard finite-size scaling: a box of side L and one of side $2L$ yields eventually the same results, as shown in Fig. 6 below. The finite range of the truncated Lennard-Jones potential (2) helps in keeping the number of interacting pairs under control even in a PBC framework.

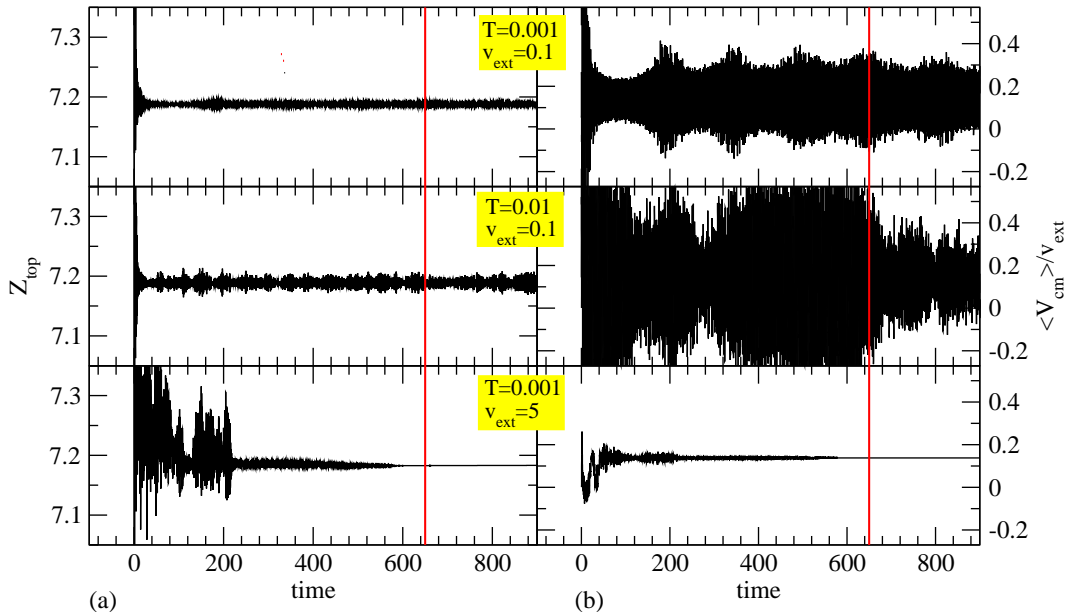


Figure 2: Position of the top layer (a) and average CM speed of the lubricant (b) as a function of time. The vertical bar locates the time (here 650 time units) which marks the end of the transient and the beginning of the stationary state, over which we compute averages. All simulations are carried out with $F = -25$. The transient detail depend on several physical quantities, such as the velocity v_{ext} of the top layer and the temperature T of the system.

3.2 Simulation Time

A simulation represents the stationary dynamical state of the system provided that the simulation time is much longer than all inner relaxation times of quantities of interest and that it provides a sufficiently long sampling of fluctuations to obtain accurate time averages. Different physical quantities have different relaxation times. Occasionally, the system tends to become slow when we consider parameters that are two or more orders of magnitude smaller or larger than the model "natural" units, since this could make it harder to reach the dynamic equilibrium under the action of some small perturbation (such as a force), so that eventually the system remains locked near its initial conditions for a longer time. This occurs, for example, at low temperature where thermal jumps do not help much reaching the expected dynamical equilibrium. In all our calculations, we must consider an initial transient, i.e. the time that the system needs to reach its dynamical stationary state. As shown in Fig. 2, the initial transient tends to be longer for low temperature simulations and for small velocity v_{ext} of the

top chain. In order to compute significant time-averages of physical quantities, we need to drop the initial transient and to consider a simulation time, at least, four or five times longer than the relaxation time of the system. A temperature increase has the effect of make all physical quantities fluctuate more around their mean values, thus we need to further increase the simulation time in order to obtain better converged averages.

4 The Plateau Dynamics

We study here the model introduced in Sect. 2, first for a single lubricant layer and then for several layers. In all cases, we consider complete layers, starting from a perfect crystalline confinement. We focus our attention on the exact velocity quantization phenomena: we find that the ratio $w = \langle v_{\text{cm}} \rangle / v_{\text{ext}}$ of the lubricant center-of-mass (CM) velocity to the externally imposed velocity of the top layer v_{ext} stays pinned to exact plateau values for wide ranges of parameters, such as v_{ext} itself, the temperature of the system and the load force F applied to the top layer. The quantized plateau occurs even with several interposed layers of lubricant. We also investigate the role of varying the top length ratio r_t . For best clarity, we consider, in all our simulations, a situation of quasi-commensuration of the chain to the bottom a_b substrate, $r_b = 1 + \delta$, with small δ : precisely we use $r_b = 29/25 = 1.16$, which produces 4 kinks every 29 lubricant particles in each layer.

4.1 Single Lubricant Layer

We illustrate here the results obtained from simulations relative to the model described in Sect. 2 with a single layer of lubricant. Figure 3 shows the time-averaged velocity $\langle v_{\text{cm}} \rangle$ of the lubricant CM, as a function of the top layer velocity v_{ext} for four vastly different temperatures of the system. The velocity ratio $w = \langle v_{\text{cm}} \rangle / v_{\text{ext}}$ is in general a complicated function of v_{ext} , with flat plateaus and regimes of continuous evolution. The main observation is that a plateau is indeed present for all but the highest temperature. To understand this plateau dynamics, Figs. 4 and 5 show the equipotential surfaces created by top and bottom atoms in a snapshot taken after the transient, with the particles moving in the plateau dynamical stationary state. As shown for the simple 1D model in [2, 3], the bottom potential, with its near-matching corrugation, is responsible for the

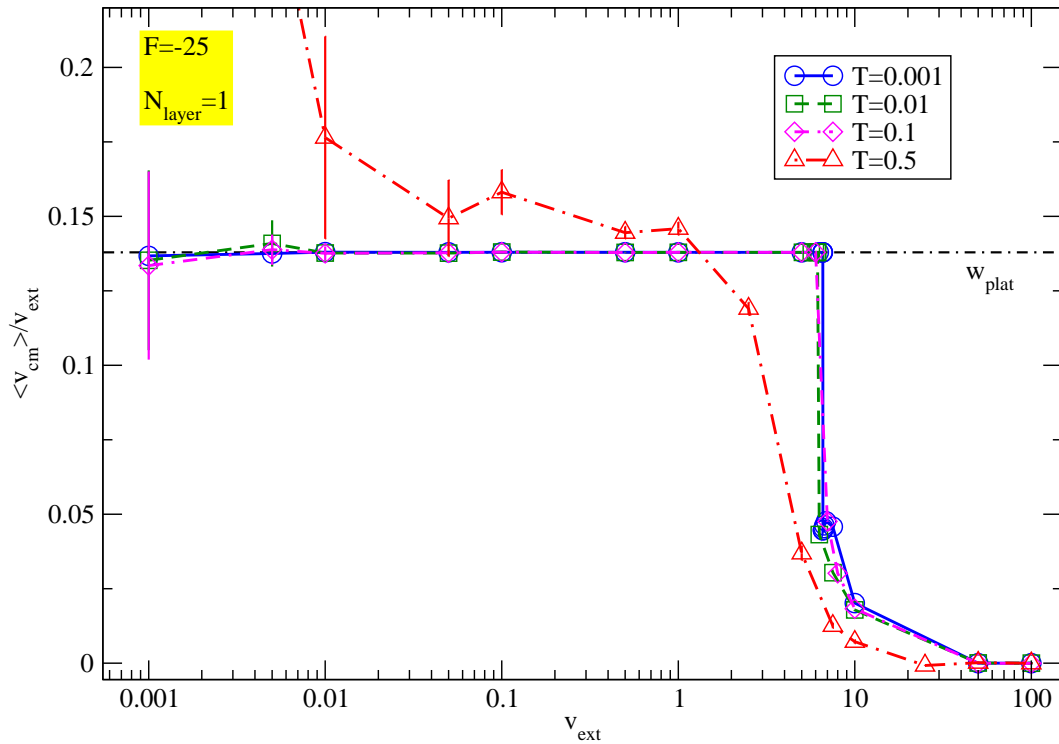


Figure 3: Average velocity ratio $w = \langle v_{\text{cm}} \rangle / v_{\text{ext}}$ of the lubricant layer as a function of the top-layer velocity v_{ext} for different temperatures. We find a plateau dynamics for all the values of temperature except for $T = 0.5$, where the system is close to melting, as the thermal energy is of the same order of magnitude as the LJ binding energy. All simulations are carried out with $F = -25$. The plateau velocity ratio is $w_{\text{plat}} = \frac{4}{29} \simeq 0.137931$.

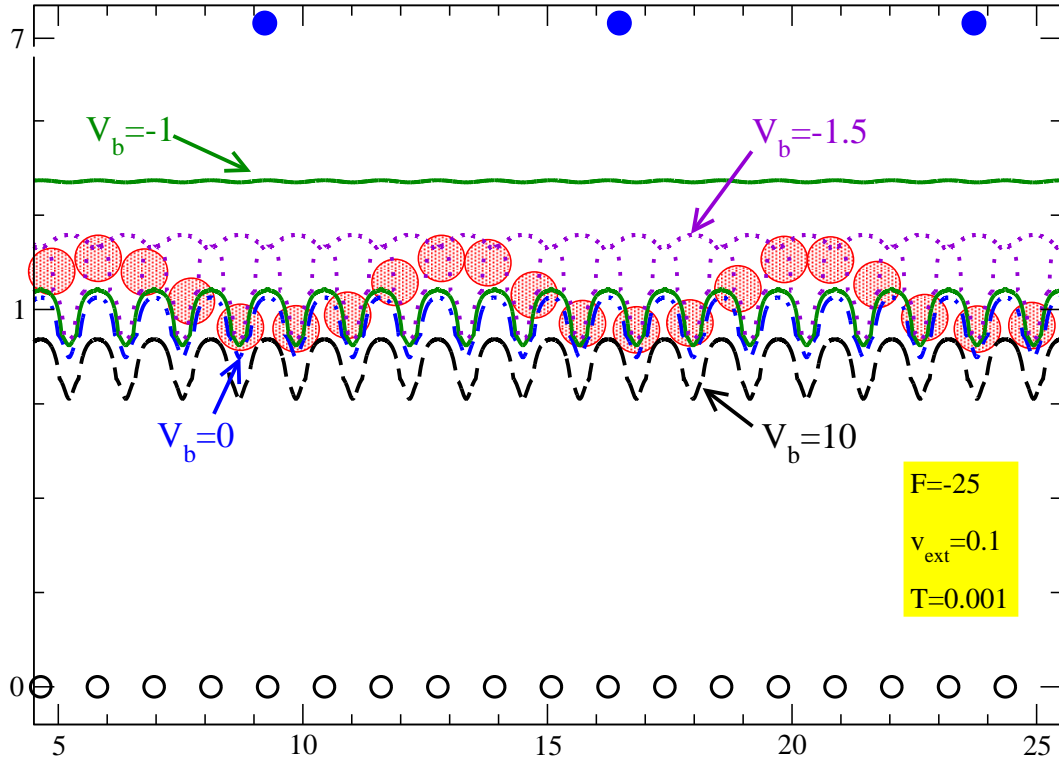


Figure 4: Equipotential surfaces for the potential energy experienced by a single lubricant particle and produced by the bottom chain. The figure reports also typical positions of bottom (open circles) and lubricant (shaded) atoms, with solitons highlighted by touching circles. The vertical displacement of the latter are induced by the interactions with the top layer atoms (solid, which surfaces are illustrated in Fig. 5 below), pressed against the lubricant by a load $F = -25$. The equipotential surfaces drawn are $V_b = 10$ (strongly repulsive), $V_b = 0$, $V_b = -1$ and $V_b = -1.5$ (strongly attractive).

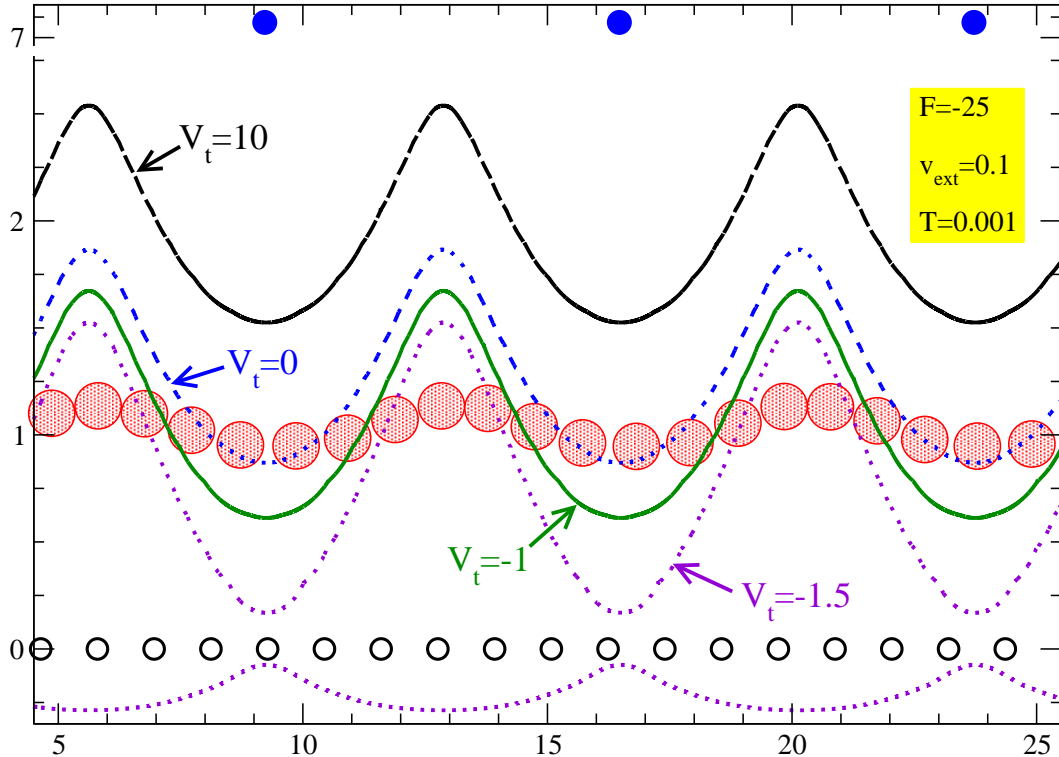


Figure 5: Equipotential surfaces for the potential energy acting on a lubricant particle, as created by the top chain (solid circles). Lubricant (shaded) and bottom (open) atoms are shown in typical positions: while the bottom potential induces kink of density ρ_{kink} , the top (which moves at fixed velocity v_{ext}) drags these kinks with velocity $v_{\text{kink}} = v_{\text{ext}}$. We see the kinks (local compressions of the chain) at the valleys (regions of $V_t \leq -1.5$) of top-potential alternated by on-register regions around saddle point regions of top potential. The deep oscillation of the top potential are responsible also for the z -displacement of the lubricant chain. The equipotential surfaces drawn are $V_t = 1$ (highly repulsive), $V_t = 0$, $V_t = -1$ and $V_t = -1.5$ (strongly attractive).

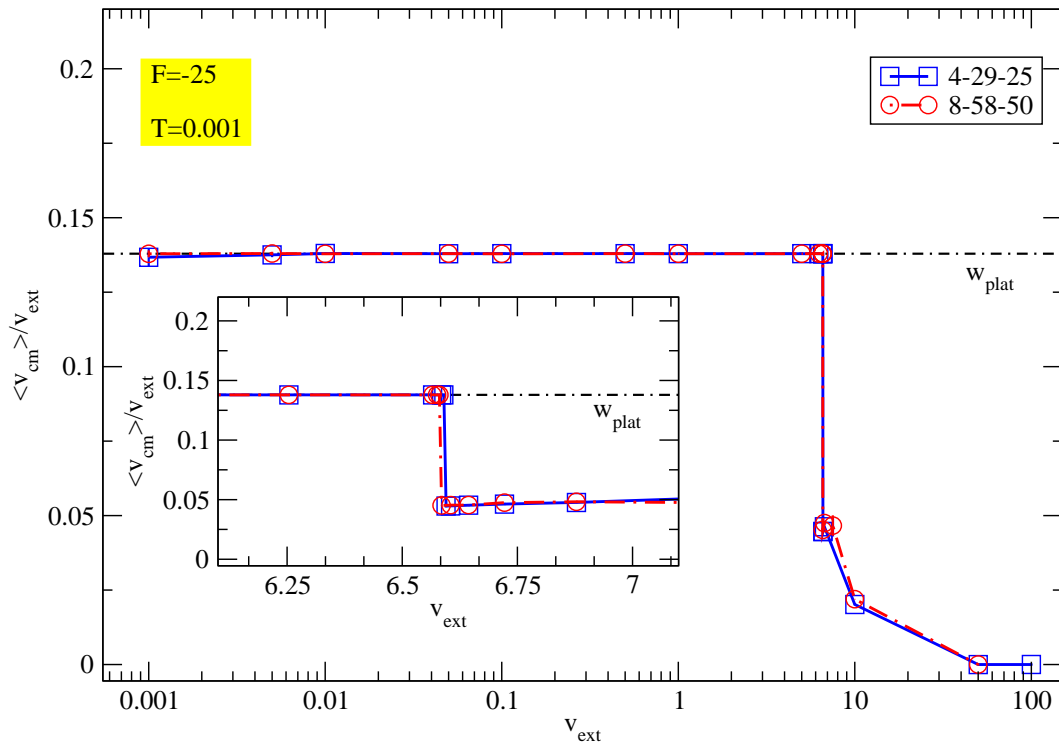


Figure 6: Finite-size scaling: we consider a box of size L (circles) and one of size $2L$ (squares) and we find the same plateau range. The box of size $L = 29a_0$ includes 4 top, 29 lubricant and 25 bottom particles. The larger box of size $L = 58$ has twice as many particles of each of the three kinds. The two lines are superimposed, showing that the dynamics is independent of the size of the box that we are considering. Inset: a blow up of the plateau edge region.

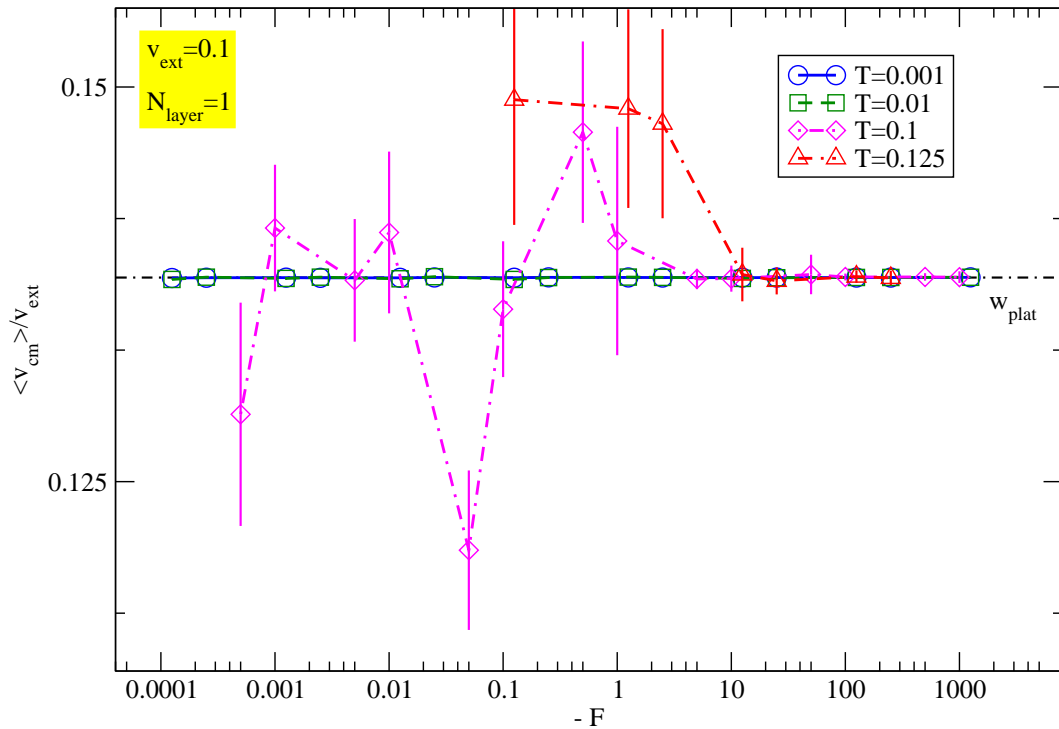


Figure 7: Average velocity ratio $w = \langle v_{\text{cm}} \rangle / v_{\text{ext}}$ of the lubricant layer as a function of the load $-F$ applied to the top particles, for different temperatures of the system. We find a strong plateau dynamics for $T = 0.001$ and $T = 0.01$, while for $T = 0.1$, only for $-F \geq 5$ and, for further increase in temperature, only for larger $|F|$, showing that the plateau benefits of a stronger load $|F|$. All simulations are carried out with $v_{\text{ext}} = 0.1$.

creation of *kinks* (or solitons), essentially local compressions of the lubricant chain with the bottom substrate potential minima holding more than one particle, see Fig. 4. As Fig. 5 shows, kinks pin to the minima of the top potential [7]. The kink density is

$$\rho_{\text{kink}} = \frac{1}{a_0} \frac{\delta}{r_b} = \frac{1}{a_0} \frac{(r_b - 1)}{r_b} = \frac{1}{a_0} \left(1 - \frac{1}{r_b}\right). \quad (19)$$

The top-layer, with its slowly oscillating potential, tends to drag the kinks along at the full speed $v_{\text{kink}} = v_{\text{ext}}$. If $\rho_0 = 1/a_0$ is the linear density of the lubricant particles, mass transport will obey $v_{\text{cm}} \rho_0 = v_{\text{kink}} \rho_{\text{kink}}$; this yields

$$w_{\text{plat}} = \frac{v_{\text{cm}}}{v_{\text{ext}}} = \frac{\rho_{\text{kink}}}{\rho_0} = 1 - \frac{1}{r_b}. \quad (20)$$

The exact plateaus arise precisely when the top substrate drags the kinks at its own full speed v_{ext} . For the length ratios of the present simulations, $w_{\text{plat}} = 4/29 \simeq 0.137931$.

As shown in Fig. 3, we find robust plateaus for a wide range of v_{ext} and for a wide range of temperature. There is evidence [3] that the plateau dynamics should extend to the limit $v_{\text{ext}} \rightarrow 0$, but it would take huge simulation time to prove within the present model. Indeed, error bars indicate increasing relative uncertainty in the determination of w for lower values of v_{ext} . For the large $T = 0.5$ we do not find any plateau dynamics: this temperature is close to melting temperature of the LJ solid [8] and the liquid lubricant does not show the plateau phenomenon. Finite-size scaling, Fig. 6, shows no size effect on the plateau boundary.

We find strong plateaus also for a wide range of load F , as shown in Fig. 7: at low temperature we find a plateau for all the values that we consider (it would become difficult investigate lower or greater load values because the simulation time would increase greatly). At large temperature, higher load is beneficial to the plateau state.

4.2 Two Lubricant Layers and Varied Kink Coverage

In the present Section, we check whether the plateau dynamics survives the presence of two layers. Figure 8 shows the typical arrangement of lubricant particles relative to the substrates in a lubricant double-layer configuration: we can still identify solitons, created by the bottom layer potential, in the lower chain, and, like for the one layer, the solitons pinned at the minima of the top potential, as in Fig. 5 for the one-layer model; the atoms of the upper lubricant layer are

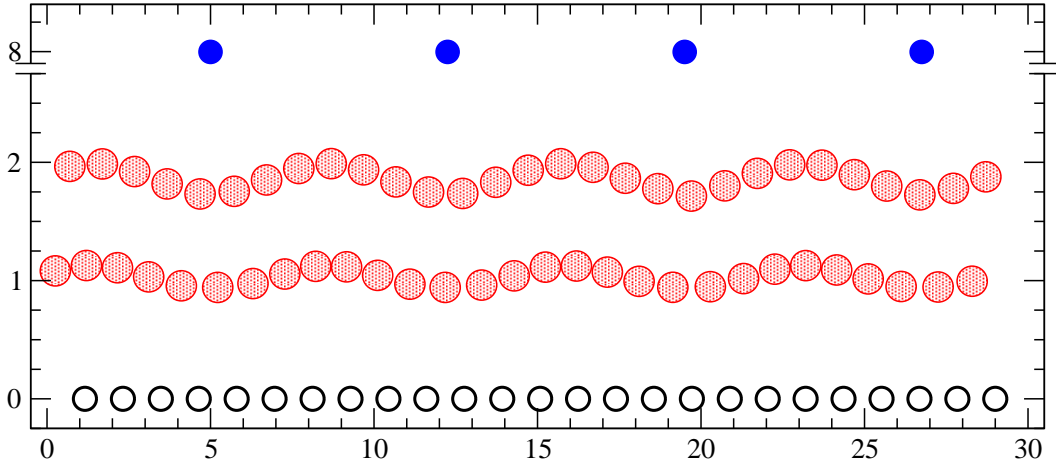


Figure 8: A sketch of the double-layer model with the top (solid circles), the lubricant (shadowed) and the bottom atoms (open). With the chosen radius of open circles, solitons are apparent as touching circles. Note that for both layers solitons arise at the same positions as in the single lubricant layer, namely near the minima of the top potential, midway between top-layer atoms.

almost equispaced. The vertical displacement for both layers is induced by the interactions with the top layer atoms.

As hinted at by Fig. 8 and shown in detail by Fig. 9, we do indeed find perfect plateau dynamics like for one lubricant chain. Thermal effects again act to destroy the plateau.

Until this point, we have chosen a situation of full commensuration of the number of kinks $N_{\text{kink}} = \rho_{\text{kink}}L$ to the number of top-atoms N_t . This is an especially favorable configuration for kink dragging, thus for the plateau phenomenon. It is then necessary to investigate situations where this full commensuration is broken. As an example of non-full commensuration, we consider 5, rather than 4, particles in the top chain, thus producing a coverage ratio $\Theta = \frac{N_{\text{kink}}}{N_t} = \left(1 - \frac{1}{r_b}\right)r_t = \frac{4}{5} = 0.8$. As shown in Fig. 10, strong plateaus occur also for $\Theta = 0.8$, both in a lubricant mono-layer and in a bi-layers. In both calculations we find a difference between the critical velocity v_{crit} at which the plateau ends. This difference is small for a single lubricant layer, while for two layers the plateau dynamics turns more fragile for a situation of imperfect commensuration $\Theta = 0.8$ than in the fully-commensurate case.

It is extremely instructive to study how v_{crit} varies when the ratio of commensuration Θ varies. We leave r_b , thus the density of solitons ρ_{kink} unchanged, while we change the number of particles in the top substrate. In Fig. 11, we plot the unpinning velocity v_{crit} as a function of the commensuration ratio Θ . We find

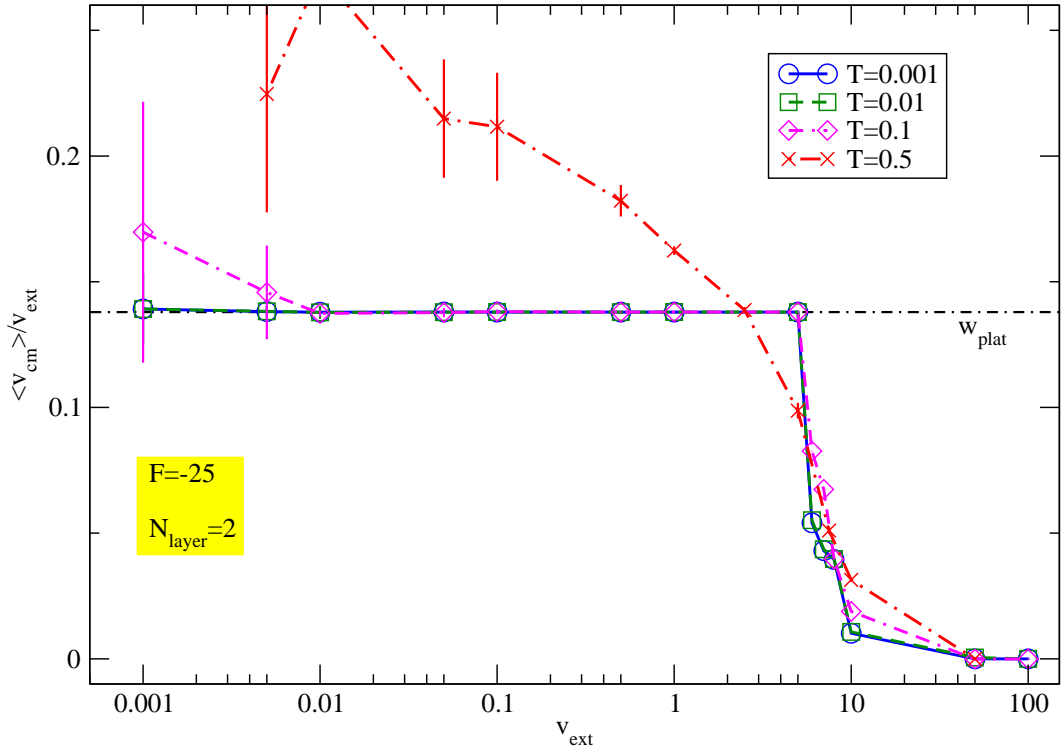


Figure 9: Two lubricant layers: average velocity ratio $w = \langle v_{\text{cm}} \rangle / v_{\text{ext}}$ of the lubricant layers as a function of the top-layer velocity v_{ext} for different temperatures of the system. Similar to the single-layer case of Fig. 3, we find a perfect plateau dynamics for moderate temperature. All simulations are carried out with $F = -25$.

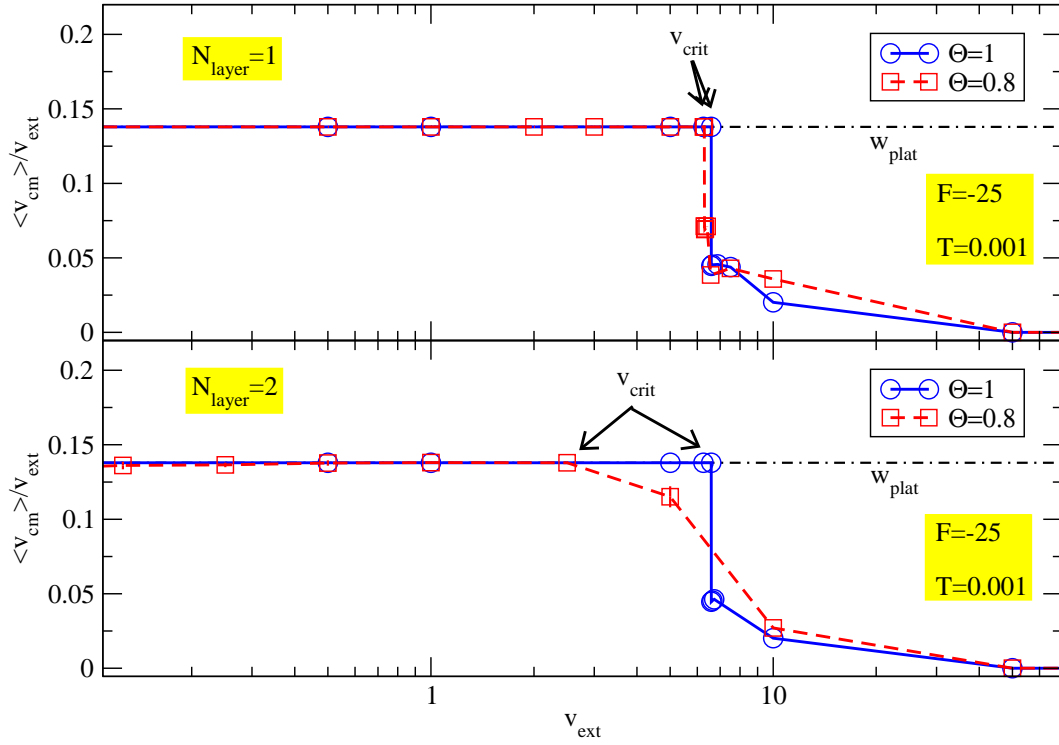


Figure 10: Comparison of the average velocity ratio $w = \langle v_{\text{cm}} \rangle / v_{\text{ext}}$ of a lubricant mono-layer and bi-layer as a function of the top-layer velocity v_{ext} for kink coverages $\Theta = 1$ and $\Theta = 0.8$. The velocity v_{crit} at which the plateau dynamics ends does depend on Θ , especially for the lubricant bi-layer where the kinks creation and dragging, thus the plateau dynamics, is more fragile.

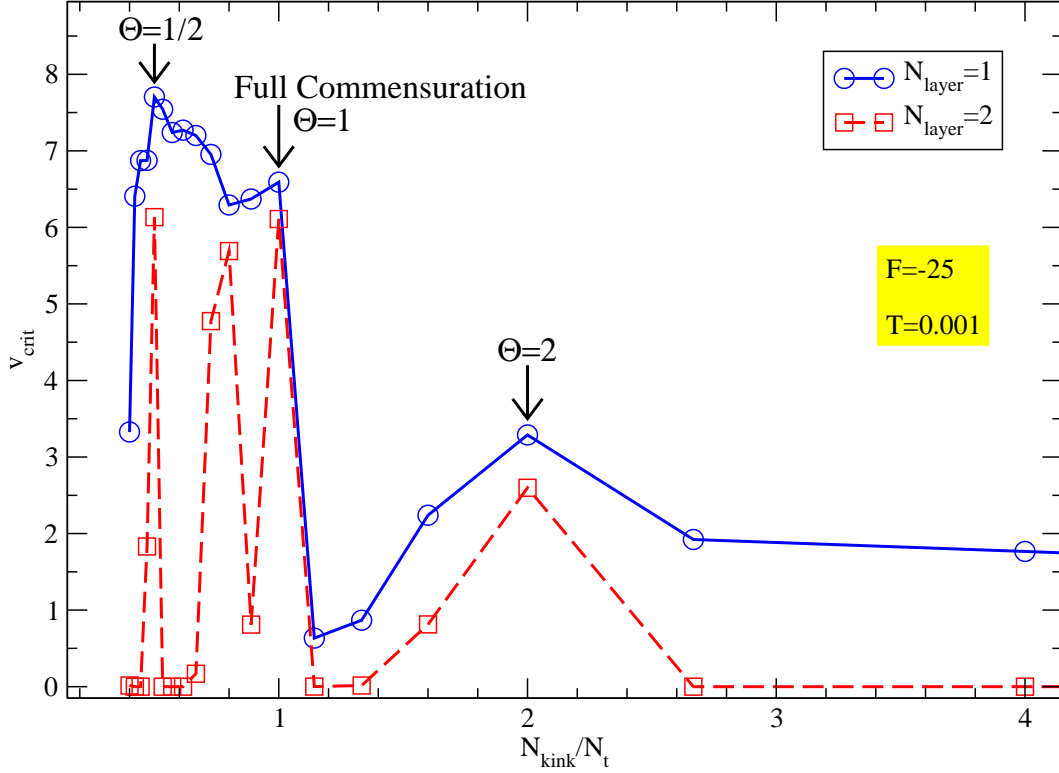


Figure 11: Variation of v_{crit} as a function of $\Theta = N_{\text{kink}}/N_t$ for the lubricant mono- and a bi-layer, always characterized by $r_b = \frac{29}{25}$. We find local maxima of v_{crit} for commensurate values of Θ for both numbers of layer, but we have stronger plateaus in the case of only one lubricant chain than in the case of two chains. The velocity for which we lose the plateau dynamics, v_{crit} , is a non trivial function of Θ . We have a local maximum for commensurable value of Θ , while for $\Theta = 1 \pm \delta$, with δ little, we have a sudden decrease of v_{crit} . All simulations are carried out with $F = -25$, $T = 0.001$ and the plateau value is $v_{\text{plat}} = \frac{4}{29} \simeq 0.137931$.

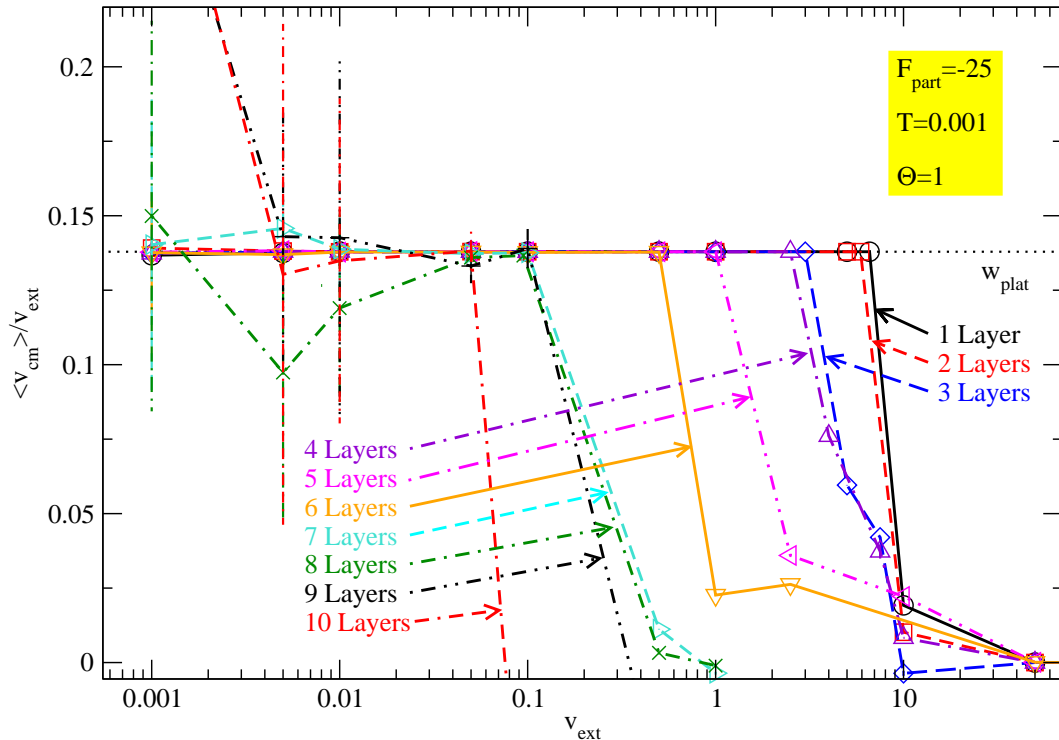


Figure 12: Average velocity ratio $w = \langle v_{\text{cm}} \rangle / v_{\text{ext}}$ as a function of the top layer velocity v_{ext} , for different numbers of lubricant solid layers. The data are consistent with a perfect plateau dynamics with up to 7 layers. v_{crit} is a decreasing function of the numbers of lubricant layers. We select a good plateau pinning configuration: $F = -25$, $T = 0.001$ and $\Theta = 1$.

local maxima for well commensurate values of Θ , both in the single and bi-layer lubricant model, but when we consider a rational value of Θ further away from full commensuration, we have a sudden decrease of v_{crit} and this drop is more drastic for two lubricant-layers than for one. For many non-integer Θ , two layers simply show no plateau even for very small v_{ext} . v_{crit} is also a function of the temperature of the system: due to thermal motion, an increase in temperature tends to reduce the strength of the plateau, thus v_{crit} .

4.3 Lubricant Multi-Layers

In Sect. 4.1 and in Sect. 4.2, we found the perfect plateau when the lubricant involves two layers. Here, as shown in Fig. 12, we insert more lubricant chains, to investigate how many layers retain the plateau dynamics. We consider a strong-

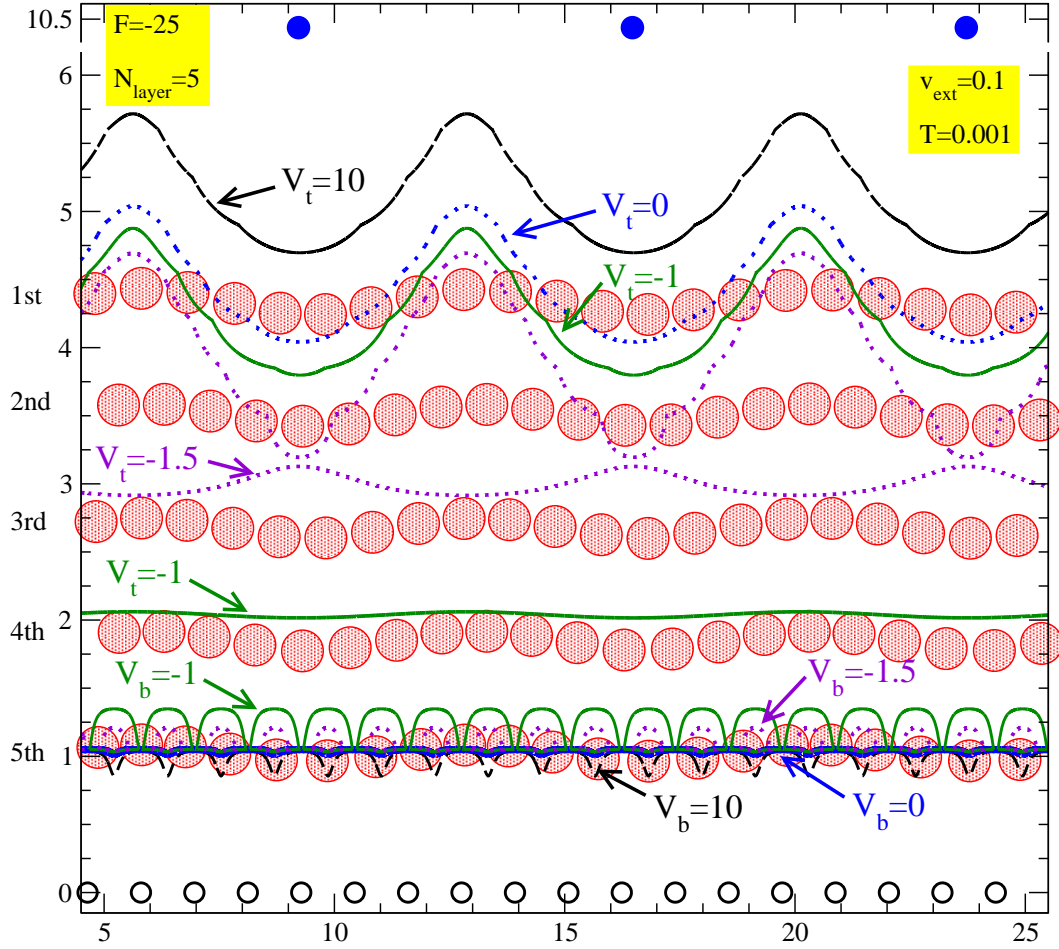


Figure 13: Equipotential surfaces for the potential energy acting on a lubricant particle, created by the top and the bottom chain for 5 lubricant layers. Top (solid circles), lubricant (shadowed) and bottom (open) atoms are shown in typical positions: the vertical displacement of all lubricant layers is induced by the interactions with the top-layer atoms, but the 5th one distants vertically mainly due to the solitonic interaction potential of the bottom substrate. The equipotential surfaces drawn for both the top and the bottom substrate are $V = 1$ (highly repulsive), $V = 0$, $V = -1$ and $V = -1.5$ (strongly attractive).

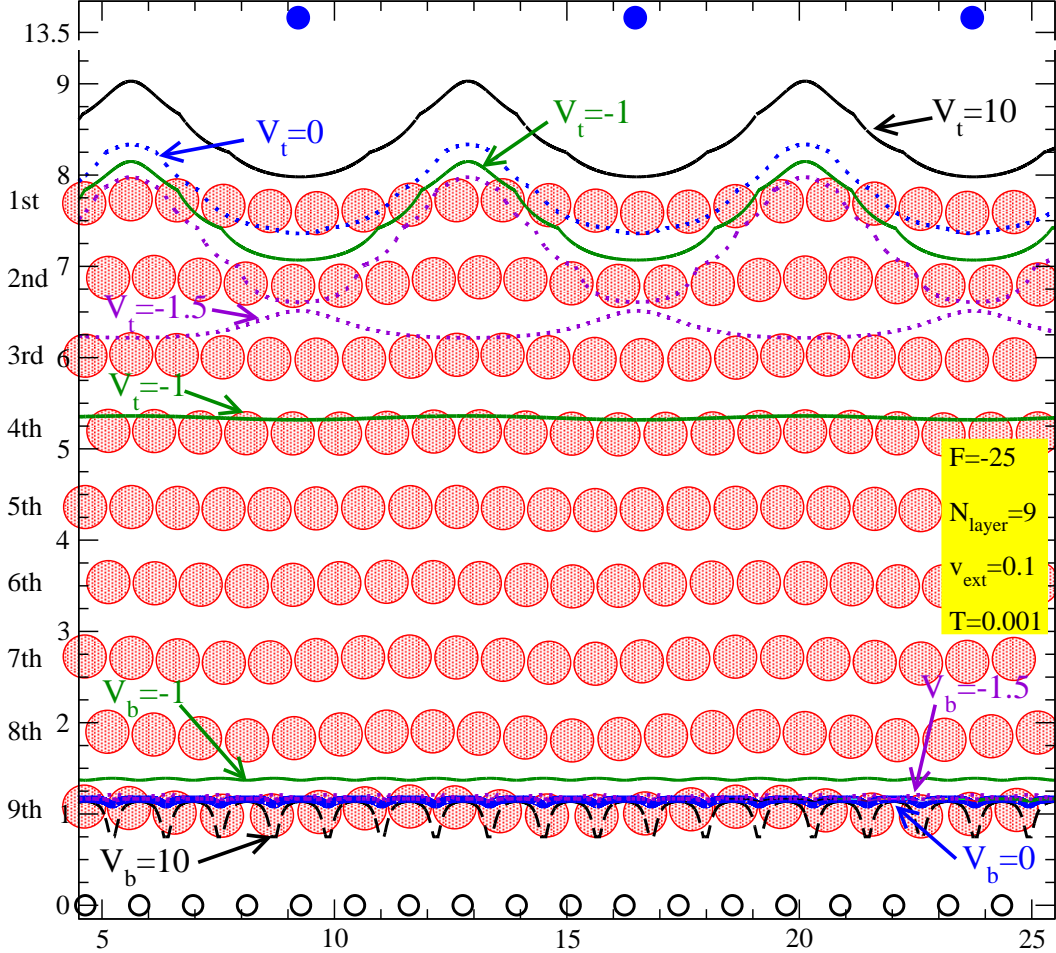


Figure 14: Equipotential surfaces for the potential energy acting on a lubricant particle, created by the top and the bottom chain for 9 lubricant layers insert. Top (solid circles), lubricant (shadowed) and bottom (open) atoms are shown in typical positions: it is clear that the vertical displacement all the layers, until the 4th, is induced by the interactions with the top layer atoms; the 5th and 6th layers are almost flat, and feel a very weakly corrugated interaction with the two substrates. Starting from the 7th layer, an increasing vertical displacement of the lubricant layers is induced initially indirectly, and then more directly by the bottom chain. The equipotential surfaces drawn are $V = 1$ (highly repulsive), $V = 0$, $V = -1$ and $V = -1.5$ (strongly attractive).

pinning condition: full kink commensuration $\Theta = 1$ with $F = -25$ and $T = 0.001$ in order to find the maximum possible number of layers capable to produce a quantized plateau velocity of the solid lubricant chain; we expect that for a weaker-pinning configuration, we should find weaker velocity plateaus compared to those that we find here. As shown in Fig. 13, the vertical displacement of the upper lubricant-layer atoms are induced by the interactions with the top layer particles, while the displacement of the lower one is induced by the potential of the bottom substrate. Although only the lowest layers interact with the bottom layer, responsible for the creation of kinks, we find a perfect plateau, at least in the limit of low v_{ext} . The cause of the z -displacement of the lubricant atoms is more evident in Fig. 14: until 4th layer, the vertical corrugation is induced by the potential of the top chain; the 5th layer is almost flat, as both the substrates are too far, their interaction with their corrugation is negligible; from the 6th layer, the chain starts to be corrugated by elastic interaction with the lubricant chain immediately below. Only the z -displacement of the 9th layer is induced directly by the bottom substrate. In a multi-layers model the solitons are created only in few layers closer to the bottom, while the atoms of the other lubricant layer are essentially equispaced. In a plateau-dynamics case, as shown in Fig. 13 the top potential and the above layers reach in and drag these solitons, while for a non-plateau case, as shown in Fig. 14, the top potential cannot move the solitons at the right velocity v_{ext} .

Figure 12 shows the progressive shift of v_{crit} to smaller values, as the number of layers increases. For several lubricant chains (up to $N_{\text{layer}} = 7$), we find perfect velocity plateaus with a decreasing v_{crit} as a function of the number of layers N_{layer} . For a further increase in N_{layer} , the top-chain slides over the higher lubricant-layer and the deeper layers experience only a small perturbation, created by the top-potential, that cannot drag the kinks created by the bottom potential. For $N_{\text{layer}} > 7$, the relaxation times become larger and larger, thus, to make simulations converge, we need longer time of simulations; this is the cause of the rather large error bars shown in Fig. 12. Even for large v_{ext} , the positions of lubricant atoms are essentially ordered and we do not find a liquid configuration, due to both the low temperature of the simulation and the full commensuration. Note that confined-induced layering and solidification is demonstrate experimentally in Ref. [9] for a few molecularly layers (typically 7, after that the lubricant becomes liquid) and analyzed theoretically in Ref. [10]. It is indeed reasonable that for a larger number of N_{layer} and even for a low v_{ext} , the top layer should not able to drag the a kinks produced by the bottom and thus the plateau dynamics disappears. Besides, as always (Fig. 3), for high temperatures, the thermal excitations make the plateau weaker.

4.4 Anti-Kinks

In the rest of Sect. 4, we set a condition of quasi-commensuration of the chain to the a_b substrate, $r_b = 1 + \delta = 1.16$, with a kink density $\rho_{\text{kink}} \simeq 4/29 a_0^{-1} = 0.137930 a_0^{-1}$. Here we consider a reversed quasi-commensurate condition that induces a kinks density $\rho_{\text{kink}} = -4/21 a_0^{-1} \simeq -0.190476 a_0^{-1}$. A positive $\rho_{\text{kink}} > 0$, induces the formation of kinks, while a negative $\rho_{\text{kink}} < 0$ produces local dilations of the chain, called *anti-kinks*, alternated to in-register regions. The anti-kinks are dragged forward at the full speed v_{ext} , since they pin to the minima of the top potential. As anti-kinks are missing particles, like holes in semiconductors, their rightward motion produces a net leftward motion of the lubricant: the lubricant chain moves in the opposite direction with respect to the top layer. As shown in Fig. 15, we find a clear reversed-velocity ($w_{\text{plat}} = -\frac{4}{21} = -0.190476$ plateau for the one-layer model). This plateau is comparably weaker, and ends at a small v_{ext} than the plateau, produces by $r_b > 1$, and shown in Fig. 3. Also two lubricant layers produce the reversed plateau at the same value of w_{plat} , but we find some evidence of another plateau for $w'_{\text{plat}} = 4/29$, that corresponds to a distance between two adjacent bottom atoms $r_b = 1.16$, i.e. the kink configuration of all previous calculations.

5 Hysteresis

We come to study the exciting bistable, hysteretic behavior found at the edge of the plateau, already found in the 1D Frenkel-Kontorova model [3, 11, 12]. We focus on the fully-commensurate $\Theta = 1$, and on the strongly-pinning configuration of parameters: $F = -25$, $T = 0.001$. Figure 16 depicts one typical such loop, obtained by cycling up and down v_{ext} in small steps, in each of which the system is let evolve for t_{calc} time units; at the next step the integration starts from the end points and velocities of the previous step, rather than from scratch as in previous Sections. The hysteretic loop is due to the meta-stable nature of the plateau state, and the finite simulation time t_{calc} being insufficient to reach its dynamic equilibrium state, such as the system is unlikely to fluctuate enough to overcome thermally a potential barrier; if t_{calc} was infinite, the system would overcome this barrier, and jump into the dynamically favored state (the plateau state below v_{crit} and the unpinned state above v_{crit}): no hysteretic loop would then appear. Of course, by increasing thermal energy even in the modest simulation times some fluctuation is likely to occur and flip the state: the hysteretic loop shrinks and

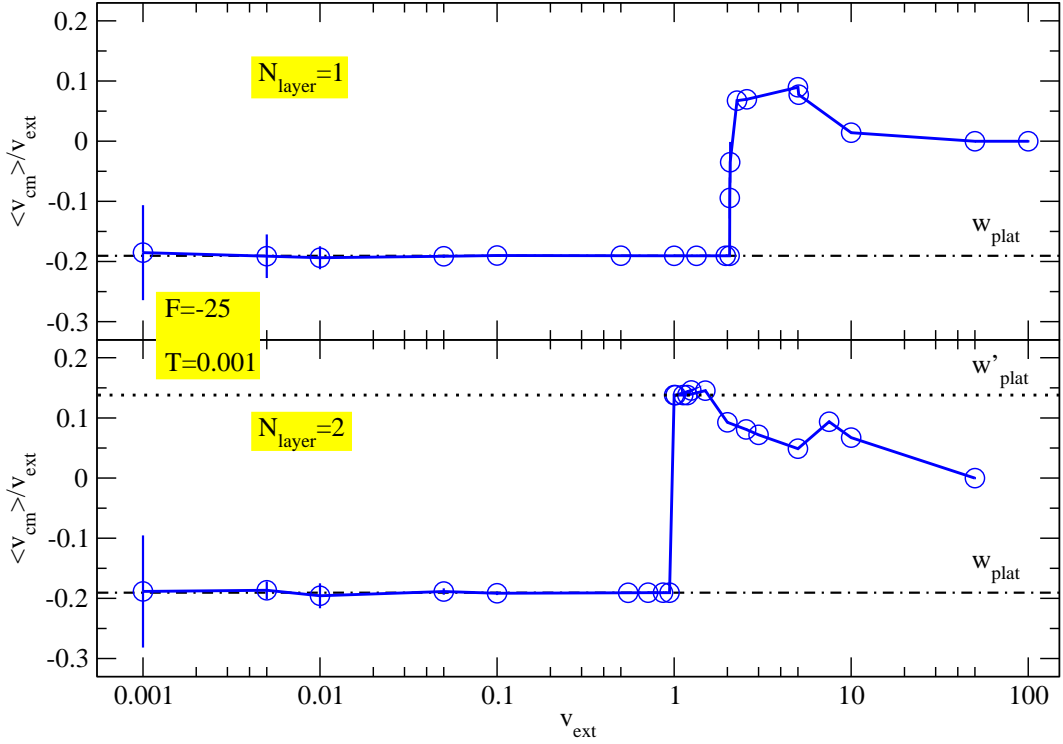


Figure 15: Average velocity ratio $w = \langle v_{\text{cm}} \rangle / v_{\text{ext}}$ as a function of the top-layer velocity v_{ext} for a model composed by 4, 21 and 25 atoms for the top, lubricant and bottom chains; these correspond to a $r_b = 21/25 = 0.84$, which according to Eq. (20), produces $w_{\text{plat}} = -\frac{4}{21} \simeq -0.190476$ (dot-dashed). Both for the one and for the two lubricant-layers, we find the perfect plateau dynamics but it is weaker than those find for $r_b = 29/25 = 1.16$. The two lubricant layers show also signs of an approximate plateau at the same value $w'_{\text{plat}} \simeq 0.137931$ of the model composed by 29 atoms for the lubricant layer and 25 for the bottom. The other simulation parameters are: $F = -25$, $T = 0.001$ and $\Theta = 1$.

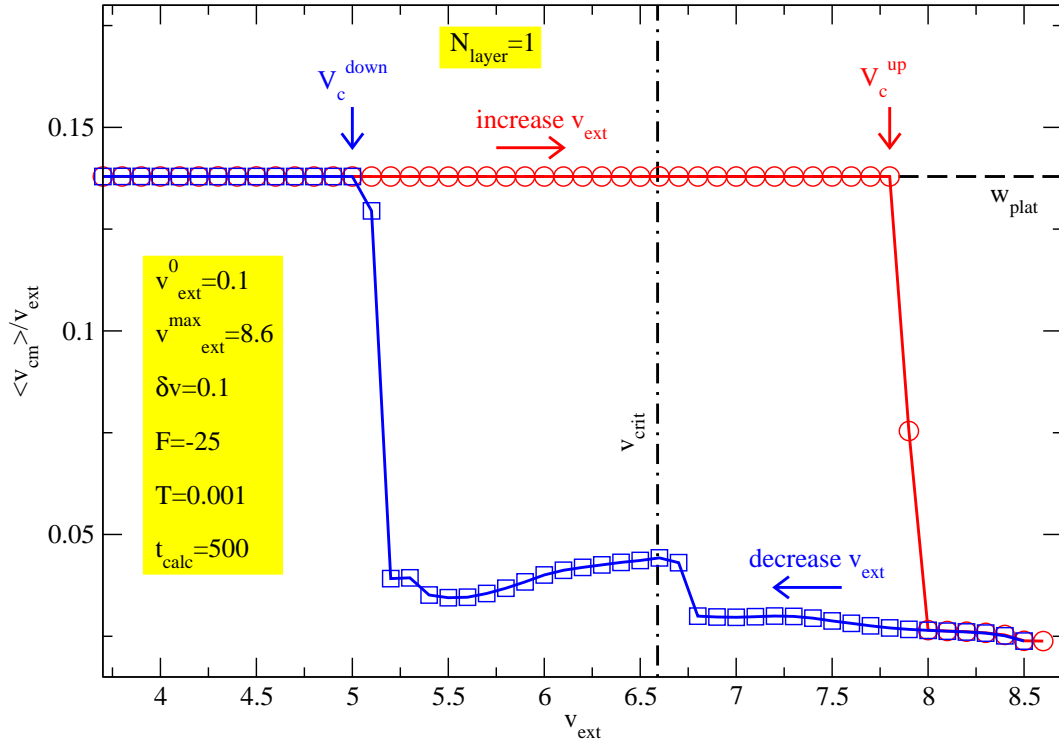


Figure 16: Average velocity ratio $w = \langle v_{cm} \rangle / v_{ext}$ as a function of the top-layer velocity when v_{ext} is cycled up and down starting from $v_{ext}^0 = 0.1$ in steps $\delta v = 0.1$ until $v_{ext}^{max} = 8.6$, each calculation being executed for $t_{calc} = 500$ time units; load $F = -25$ and $T = 0.001$. Increase and decrease of v_{ext} is denoted by circles and squares respectively. The critical velocity $v_{crit} \simeq 6.59$ obtained as described in Sect. 4.2, is marked by a dot-dashed line.

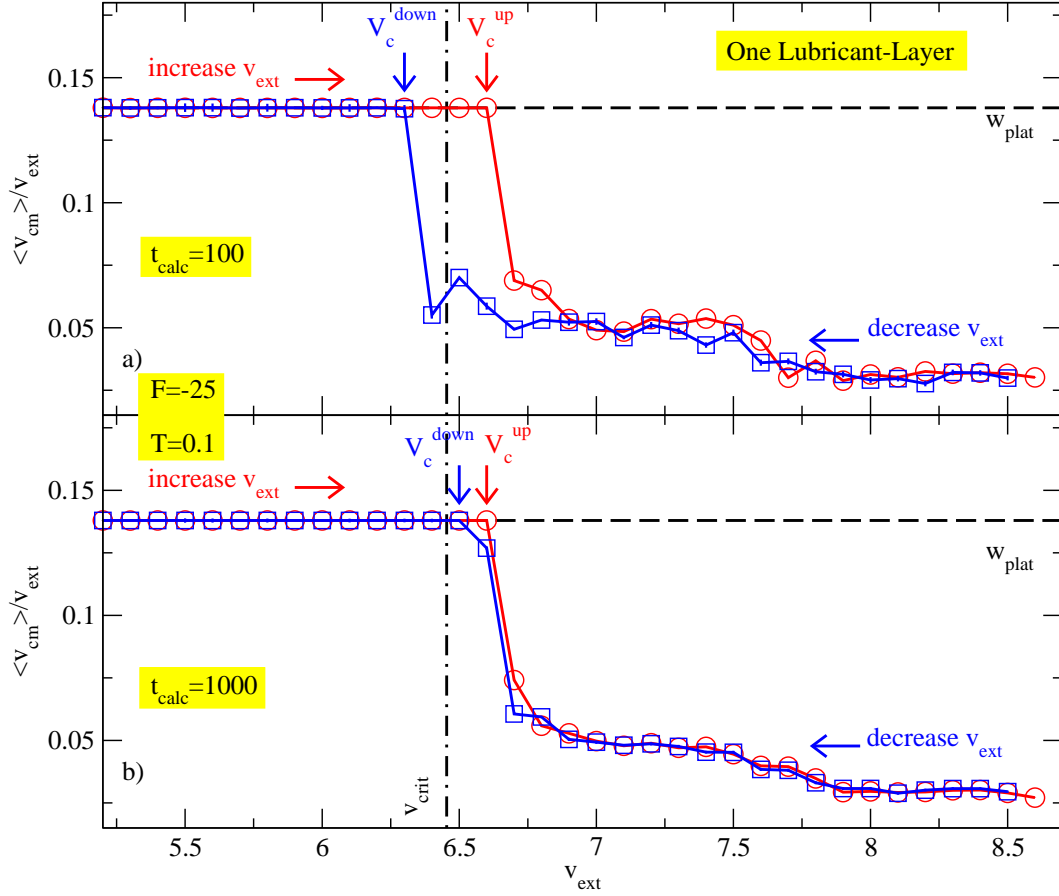


Figure 17: Average velocity ratio $w = \langle v_{\text{cm}} \rangle / v_{\text{ext}}$ as a function of top-layer's velocity when v_{ext} is cycled. Increase and decrease of v_{ext} is denoted by circles and squares respectively. *a)* $t_{\text{calc}} = 100$ an hysteretic loop appears; *b)* $t_{\text{calc}} = 1000$, comparable to or larger than the system relaxation time, so that the hysteretic loop almost closes. The simulations are carried out at $T = 0.1$. The plateau velocity is $w_{\text{plat}} = \frac{4}{29} \simeq 0.137931$ and the critical velocity obtained by simulations where all calculations restart from scratch is $v_{\text{crit}} \simeq 6.45$.

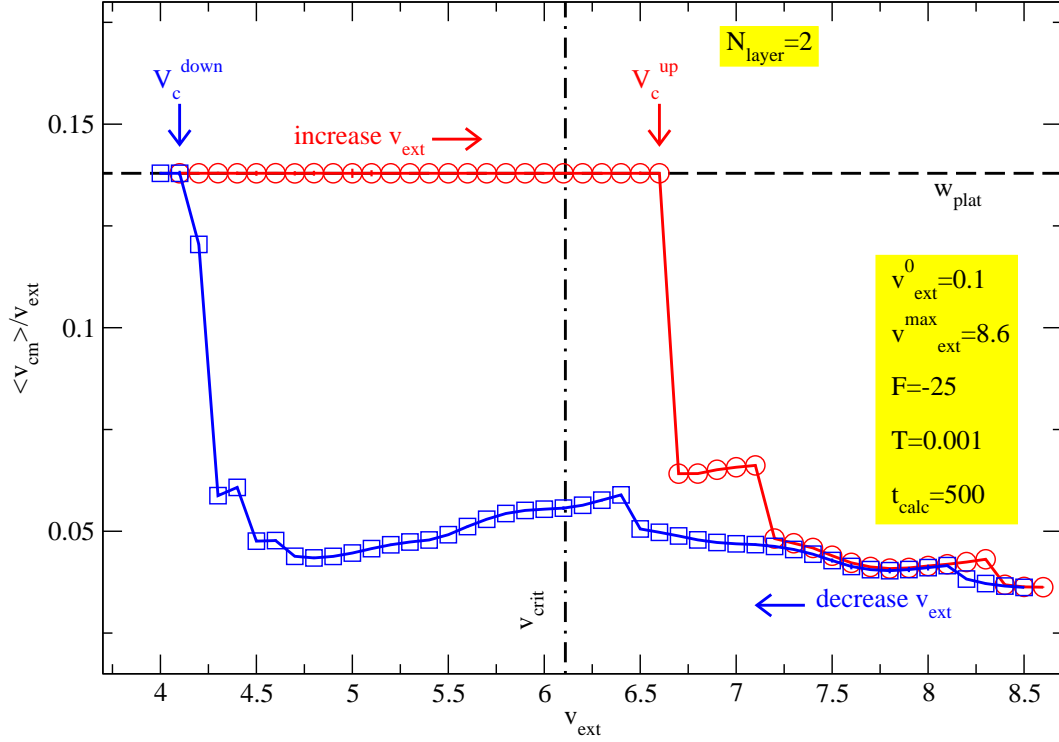


Figure 18: Average velocity ratio $w = \langle v_{cm} \rangle / v_{ext}$ when v_{ext} is cycled in steps $\delta v = 0.1$. Increase and decrease of v_{ext} is denoted by circles and squares respectively. Here we insert two lubricant layers among the top and the bottom-chains. The simulations are carried out at $T = 0.001$. The hysteric loop is even wider than the one-layer loop of Fig. 16 because the system needs longer to reach the dynamical stationary state. The plateau velocity is $w_{plat} = \frac{4}{29} \simeq 0.137931$ and the critical velocity determined by restarting each calculation from scratch is $v_{crit} \simeq 6.12$.

eventually closes.

Within these theoretical limitations, in practice at not too large temperature (e.g. $T = 0.001$ as in Fig. 16), for any practically conceivable simulation time the hysteretic plateau boundary is a very clear reality: the plateau dynamics is only abandoned above a critical velocity $v_c^{\text{up}} > v_{\text{crit}}$; when v_{ext} is reduced back, the depinned state survives below v_{crit} to a smaller $v_c^{\text{down}} < v_{\text{crit}}$ where the plateau dynamics is retrieved. Due to the reasons mentioned above, the detailed values of v_c^{up} and v_c^{down} are functions of t_{calc} (beside the physical model parameters), but in practice a very slowly varying function.

Figure 17 shows the hysteretic loop for two simulations carried out at the same conditions as for Fig. 16, except for a comparably large temperature $T = 0.1$, and with different duration of each velocity increase step, in panel (a) with $t_{\text{calc}} = 100$ and in (b) with $t_{\text{calc}} = 1000$: in Fig. 17b, the time of each simulation is ten times larger than that of Fig. 17a, so that each simulation has a larger probability to decay from the meta-stable state and reach the dynamical stationary state most suitable for that value of v_{ext} . The hysteresis loop that appearing in a $T = 0.1$ -simulations is narrower than that of $T = 0.001$ because wider and more frequent thermal fluctuations. Figure 18 shows an hysteretic loop also for two lubricant layers: the hysteresis is even wider than for one layer, indicating higher energy barriers and layer relaxation times than for one layer.

6 Analysis of the Fluctuations

Interesting informations can be gathered through the analysis of the fluctuations of the physical quantities around their stationary values in the plateau state. For example, Fig. 19 reports the comparison of the fluctuations of r_z^{top} with those of the lubricant CM \hat{x} -velocity v_{cm} . The two quantities show modest correlations, as clarified by the correlation sampling of Fig. 20.

These fluctuations can be analyzed by Fourier spectral techniques, as we do in Fig. 21 for the fluctuations of r_z^{top} in a single lubricant model with $F = -25$, $v_{\text{ext}} = 0.5$ and $T = 0.001$: beside some low-frequency and high-frequency noise, we observe a remarkable peak at frequency $\nu \simeq 0.4$ and multiples with its harmonic. To understand the nature of this $\nu \simeq 0.4$ peak, we first (Fig. 22a) rule out the possibility that it is related to the top layer encountering the lubricant "bumps". In fact, we find this frequency completely unchanged when we change v_{ext} by a large factor. To rule out the possibility that the $\nu \simeq 0.4$ peak may be the natural vertical oscillation of top chain around its average value due to the force applied

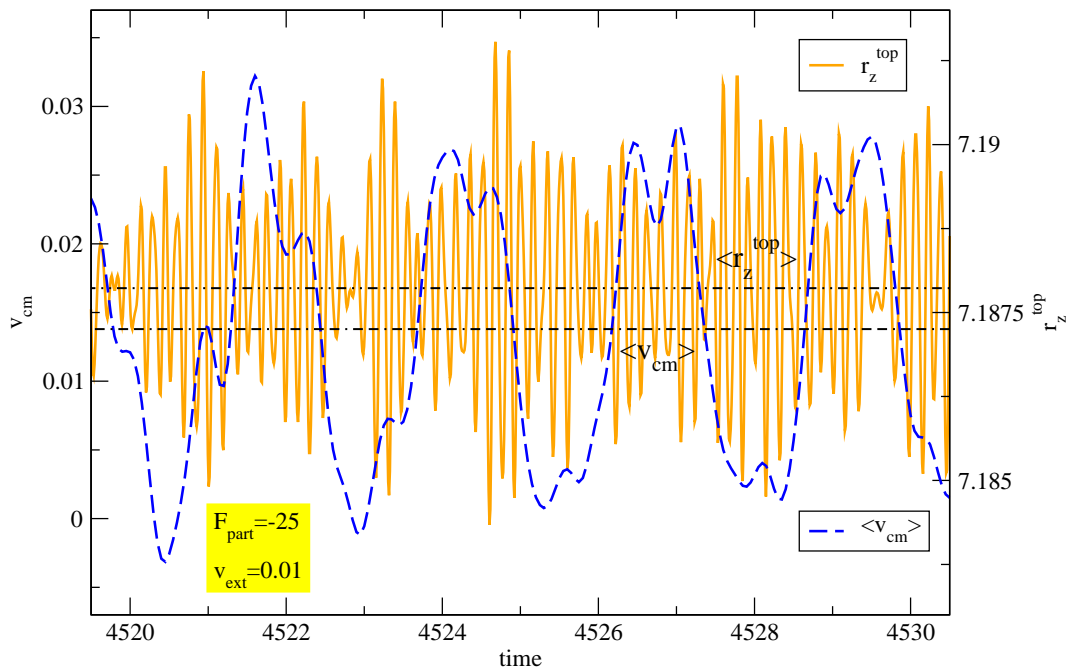


Figure 19: Position along the z -axis of the top layer (solid) and lubricant CM velocity v_{cm} (dashed) as a function of time. The simulation is carried out at coverage $\Theta = 1$, load $F = -25$ and sliding speed $v_{\text{ext}} = 0.01$. v_{cm} fluctuates around $\langle v_{\text{cm}} \rangle = w_{\text{plat}} v_{\text{ext}} \simeq 0.01379$. The average value of the position of top-layer is $\langle r_z^{\text{top}} \rangle \simeq 7.19$.

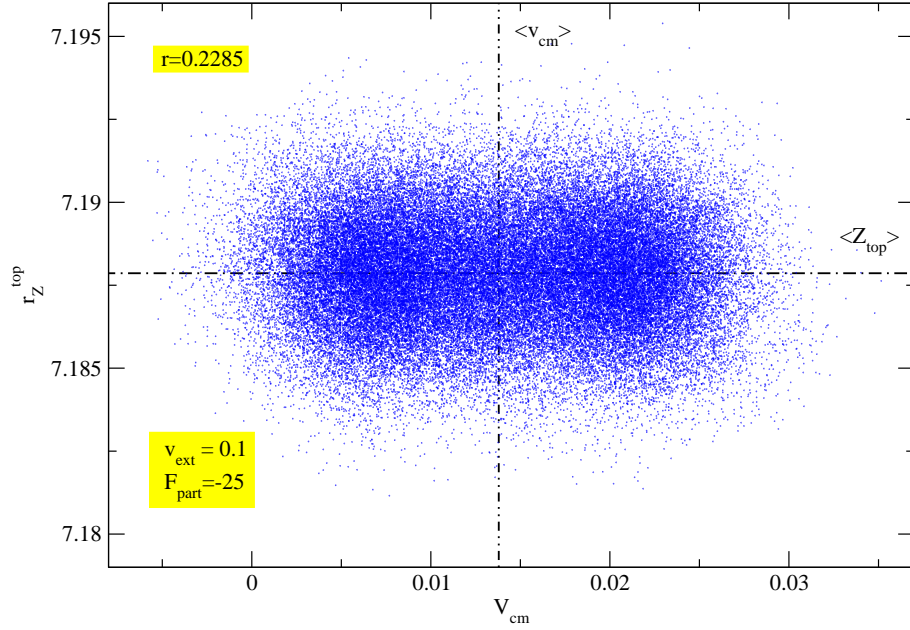


Figure 20: Correlation between the z -position of the top layer and the value of lubricant CM velocity. The correlation coefficient is $r = 0.2285$.

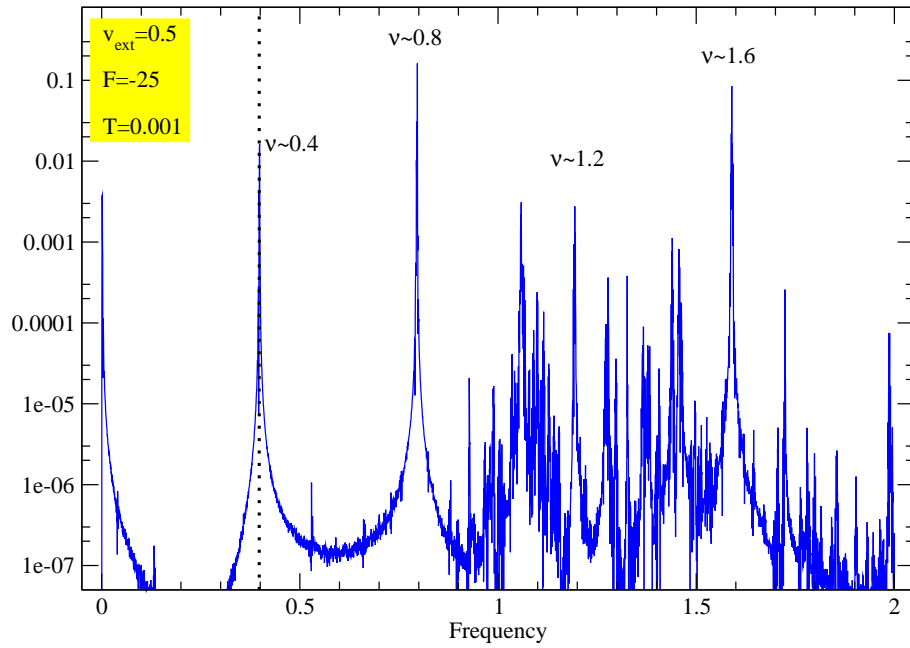


Figure 21: Fourier analysis of the oscillation of z -position of the top chain for one lubricant-layer model with $F = -25$, $v_{\text{ext}} = 0.5$ and $T = 0.001$. In the figure, appears some peaks at $\nu \simeq 0.4$ and multiples and big noise frequencies from $\nu \simeq 1$ to $\nu \simeq 2$.

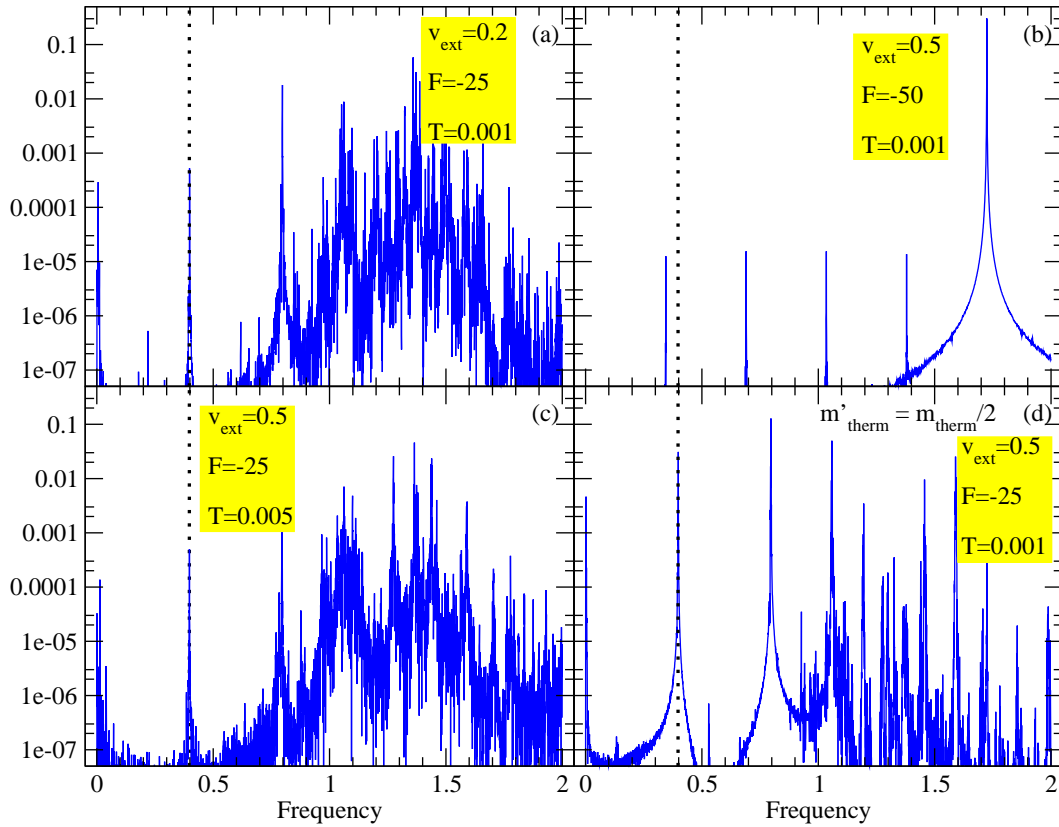


Figure 22: Fourier analysis of the oscillation of z -position of the top chain. In order to discover what are the causes of the peaks and noise of Fig. 21, we start from the parameters of Fig. 21 and change v_{ext} in Fig. 22a; F in Fig. 22b; T in Fig. 22c and m_{therm} in Fig. 22d. The vertically-dotted lines indicated the frequency ν finds in Fig. 21.

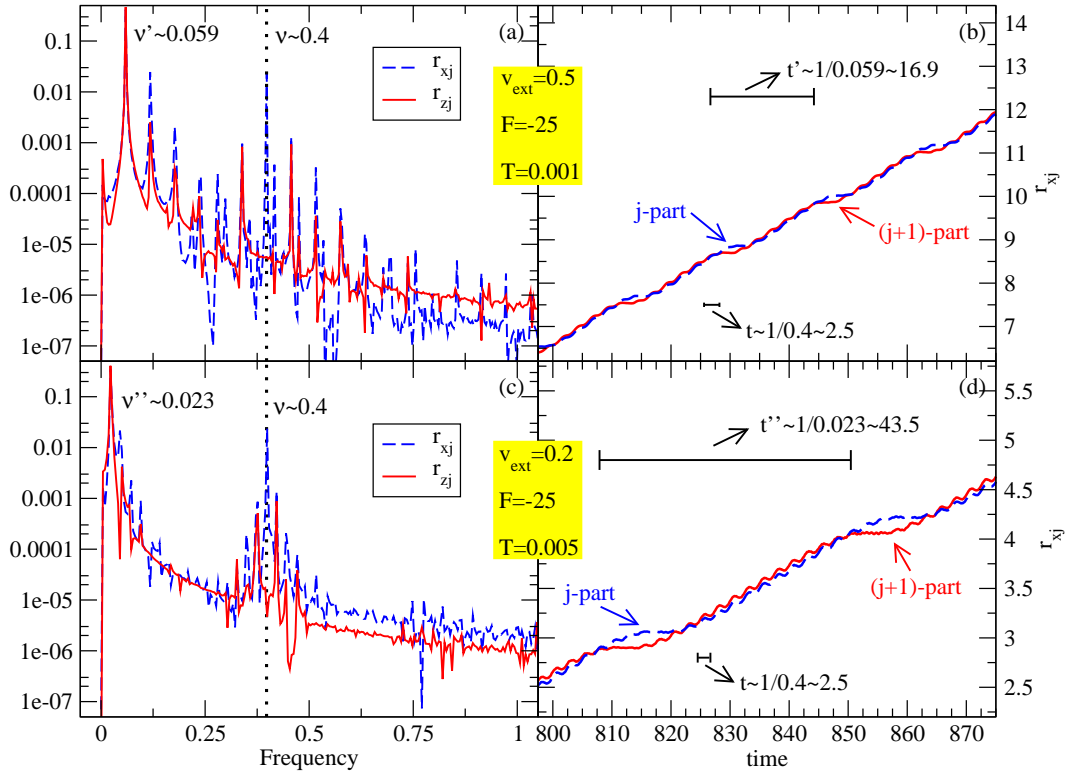


Figure 23: In *a* and *c*, Fourier analysis of the oscillation of x - (dashed line) and z -position (solid) of a lubricant particle for $v_{\text{ext}} = 0.5$ and $v_{\text{ext}} = 0.2$ respectively. In *b* and *d*, the positions of two adjacent particles of the lubricant chain as a function of time. We find peaks at ν only for the fluctuations of the x -position.

over the top and to the repulsive forces of potentials (1), in Fig. 22*b* we increase F by a factor 2 and find the same peaks of Fig. 21 shifted to a slightly lower (rather than higher!) frequency $\nu \simeq 0.345$ and its multiples. We also rule out that there is an unphysical oscillation related to energy exchange with the Nosé-Hoover thermostat, by changing the temperature T of the simulation (Fig. 22*c*), or the mass of the thermostat m_{therm} , tuning the thermostat responsiveness (Fig. 22*d*): no significant changes relative to Fig. 21. We obtain some insight about the physical nature of the $\nu \simeq 0.4$ by analyzing the fluctuations of the x - and z -positions of a generic particle j of the lubricant chain. As shown in Fig. 23*a* (solid line), the x motion contains the same frequency $\nu \simeq 0.4$ as r_z^{top} (Fig. 21) plus a peak at $\nu' \simeq 0.059$. ν' is related to the period $T' \simeq 16.96$ between two stops of Fig. 23*b*, while the frequency $\nu \simeq 0.4$ is linked with the rapid oscillations that elapse between successive stops. The stop marks the moment when the particle fits in between two atoms of the bottom substrate, while the stairway part indicates the interval when a particle belongs to a kink. Comparing two adjacent particles (Fig. 23*b* and *d*), we see that their x -movement is in phase, thus indicating acoustic modes. Compare Fig. 23*a* and *b* ($v_{\text{ext}} = 0.5$), with Fig. 23*c* and *d* ($v_{\text{ext}} = 0.2$): we see the same phonon $\nu \simeq 0.4$, while the ν' shifts to $\nu'' \simeq 0.023$ (period $t'' \simeq 44.11$) corresponding to the increased time interval between successive stops. Remarkably, no sign of ν' is seen in the r_z^{top} spectrum, while the frequency $\nu \simeq 0.4$ of a "horizontal" lubricant vibration adds coherently and is seen in the "vertical" fluctuation of the top layer. The solid curves of Fig. 23*a* and *c* shown the Fourier analysis of the z -position of the particle: we find the same frequency ν' and thus the same period that elapses between two stops, but no sign of the frequency ν , which is therefore a purely longitudinal mode.

7 Discussion and Conclusion

Within the idealized scheme of a simple 1D Frenkel-Kontorova-like model, a special "quantized" sliding state was found for a solid lubricant confined between two periodic layers [1]. This state, characterized by a nontrivial geometrically fixed ratio of the mean lubricant drift velocity $\langle v_{\text{cm}} \rangle$ and the externally imposed translational velocity v_{ext} , was understood as due to the kinks (or solitons), formed by the lubricant due to incommensuration with one of the substrates, pinning to the other sliding substrate.

In the present work, a quantized sliding state of the same nature is demon-

strated for a substantially less idealized 2D model, where atoms are allowed to move perpendicularly to the sliding direction and interact via Lennard-Jones potentials. At first, we analyze the single lubricant layer model for varied driving speed v_{ext} and we find perfect plateaus, at the same geometrically determined velocity ratio w_{plat} as observed in the simple 1D model, not only at low temperatures, but also for temperatures not too far from a melting point of the LJ lubricant. An increased load- F is beneficial to the plateau state at high temperature. The velocity plateau, as a function of v_{ext} , ends at a critical velocity v_{crit} , and for $v_{\text{ext}} > v_{\text{crit}}$ the lubricant moves at a speed which is generally lower than that of the plateau state. In fact, by cycling v_{ext} , the layer sliding velocity exhibits an hysteretic loop around v_{crit} . For a bi-layer model, we find very similar results as for one layer. The unpinning velocity v_{crit} is linked to the rate of commensuration Θ : local maxima are located at well-commensurate Θ values. The plateau dynamics is found even with a confined solid lubricant composed of multiple (up to 7) lubricant layers: the strength of the plateau (measured by v_{crit}) is a decreasing function of the number of layers. Characteristic backward lubricant motion produced by the presence of "anti-kinks" is also shown in this context. The present work focuses on ordered configurations: both substrate are perfect crystals and the lubricant retains the configuration of a strained crystalline solid. It will be the object of future investigation the role of disorder both in the substrate [13] and in the lubricant. The analysis of friction itself and the significance of fluctuations in the dynamical properties will also require further study.

References

- [1] N. Manini, M. Cesaratto, G. E. Santoro, E. Tosatti, and A. Vanossi, *J. Phys.: Condens. Matter* **19**, 305016 (2007).
- [2] A. Vanossi, N. Manini, G. Divitini, G. E. Santoro and E. Tosatti, *Phys. Rev. Lett.* **97**, 056101 (2006).
- [3] N. Manini, G. E. Santoro, E. Tosatti, and A. Vanossi, *Phys. Rev. E* **76**, 046603 (2007).
- [4] D. Frenkel and B. Smit, *Understanding Molecular Simulation. From Algorithms to Applications* (Academic Press, 1996).
- [5] G. J. Martyna, M. L. Klein and M. Tuckerman, *J. Chem. Phys.* **97**, 2635 (1992).
- [6] W. H. Press, S. A. Teukolsky, W. T. Vetterling and B. P. Flannery, *Numerical Recipes in Fortran. The Art of Parallel Scientific Computing* (Cambridge University Press, 1996).
- [7] O. M. Braun and Y. S. Kivshar, *The Frenkel-Kontorova Model: Concepts, Methods, and Applications* (Springer-Verlag, Berlin, 2004).
- [8] S. Ranganathan and K. N. Pathak, *Phys. Rev. A* **45**, 5789 (1992).
- [9] J. Klein and E. Kumacheva, *J. Chem. Phys.* **108**, 6996 (1998).
- [10] B. N. J. Persson, *Surf. Sci. Rep.* **33**, 83 (1999).
- [11] A. Vanossi, G. E. Santoro, N. Manini, M. Cesaratto, and E. Tosatti, *Surf. Sci.* **601**, 3670 (2007).
- [12] A. Vanossi, N. Manini, F. Caruso, G. E. Santoro, and E. Tosatti, arXiv:0709.3706 [cond-mat.mtrl-sci], in print in *Phys. Rev. Lett.* (2007).
- [13] R. Guerra, A. Vanossi, M. Ferrario, *Surf. Sci.* **601**, 3676 (2007).